Quantitative temperature monitoring of a heat tracing experiment using cross-borehole ERT

Hermans Thomas[1,2], **Wildemeersch Samuel**[3], **Jamin Pierre**[3], **Orban Philippe**[3], **Brouyère Serge**[3], **Dassargues Alain**[3], **Nguyen Frédéric**[1].

[1]University of Liege, Applied Geophysics, Department ArGEnCo, Engineering Faculty, B52, 4000 Liege, Belgium.

[2]F.R.S.-FNRS Research Fellow.

[3]University of Liege, Hydrogeology and Environmental Geology, Aquapole, Departement ArGEnCo, Engineering Faculty, B52, 4000 Liege, Belgium.

Corresponding author

Hermans Thomas, University of Liege, Applied Geophysics, Department ArGEnCo, Engineering Faculty, B52, Chemin des Chevreuils 1, 4000 Liege, Belgium. Tel : +3243669263, Fax : +3243669520, thomas.hermans@ulg.ac.be

:Hermans T., S. Wildemeersch., P. Jamin, P. Orban, S. Brouyère, A. Dassargues and F. Nguyen. 2015. Quantitative temperature monitoring of a heat tracing experiment using cross-borehole ERT. *Geothermics*, 53, 14-26. doi: http://dx.doi.org/10.1016/j.geothermics.2014.03.013

Abstract

The growing demand for renewable energy leads to an increase in the development of geothermal energy projects and heat has become a common tracer in hydrology and hydrogeology. Designing geothermal systems requires a multidisciplinary approach including geological and hydrogeological aspects. In this context, electrical resistivity tomography (ERT) can bring relevant, qualitative and quantitative information on the temperature distribution in operating shallow geothermal systems or during heat tracing experiments. We followed a heat tracing experiment in an alluvial aquifer using cross-borehole time-lapse ERT. Heated water was injected in a well while water of the aquifer was extracted at another well. An ERT section was set up across the main flow direction. The results of ERT were transformed into temperature using calibrated petrophysical relationships. These ERT-derived temperatures were then compared to direct temperature measurements in control piezometers collected with distributed temperature sensing (DTS) and groundwater temperature loggers. Spatially, it enabled to map the horizontal and vertical extent of the heated water plume, as well as the zones where maximum temperatures occurred. Quantitatively, the temperatures and breakthrough curves estimated from ERT were in good agreement with the ones observed directly during the rise and maximum of the curve. An overestimation, likely related to 3D effects, was observed for the tail of the heat breakthrough curve. The error made on temperature can be estimated to be between 10 to 20 %, which is a fair value for indirect measurements. From our data, we estimated a quantification threshold for temperature variation of 1.2°C. These results suggest that ERT should be considered when designing heat tracing experiments or geothermal systems. It could help also to assess the geometrical complexity of the concerned reservoirs. It also appears that ERT could be a useful tool to monitor and control geothermal systems once they are in operation.

Keywords: Heat tracing, geothermal system, time-lapse, cross-borehole electrical resistivity tomography, temperature monitoring

1. Introduction

Shallow alluvial aquifers constitute potential shallow geothermal energy reservoirs, relatively abundant and easily accessible. In these low temperature systems, groundwater has an average temperature ranging from 5 to 30°C and may be used for domestic or industrial cooling and heating (Allen and Milenic, 2003; Haehnlein et al., 2010).

The two main techniques to exploit shallow geothermal energy systems are ground source heat pump (GSHP), which are closed systems with a vertical or horizontal heat exchanger, and groundwater heat pump (GWHP), which are open systems circulating groundwater between production and injection wells. Designing such systems requires a multidisciplinary approach including geological and hydrogeological aspects. The most common approach is to model the system using a coupled groundwater and heat flow simulator. However, such models require estimating parameters governing heat transport such as heat capacity, thermal conductivity and density. Due to a lack of data, authors often have to rely on standard calculation charts, values found in the literature or default values implemented in softwares (e.g. Busby et al., 2009; Lo Russo and Civita, 2009; Liang et al., 2011; de Paly et al., 2012). In-situ tests, such as thermal response tests (Raymond et al., 2011; Mattsson et al., 2008), or laboratory measurements (e.g. Haffen et al., 2013) are sometimes possible but the deduced values may deliver only well-centered information or may not always be representative of in-situ conditions.

Thermal tracing experiments are performed for decades in hydrogeology (Anderson, 2005; Saar, 2011). Such experiments are used to improve the characterization of hydrogeological parameters (e.g. hydraulic conductivity or dispersivity), but the same methodologies may be used to study the thermal properties of shallow geothermal systems (e.g. Vandenbohede et al., 2009, 2011; Giambastiani et al. 2012). However, the heterogeneity of geothermal and hydrogeological systems may be too complex to be fully caught by thermal or solute tracer experiments alone (e.g. Brouyère, 2001).

In this context, electrical resistivity tomography (ERT) can bring relevant and spatially distributed information both on the heterogeneity of aquifers and on the temporal behavior of tracers. Indeed, ERT has proven its efficiency to image and/or monitor spatial phenomena (Vereecken et al., 2006) such as salt water intrusions (Nguyen et al., 2009; Hermans et al., 2012c), variations in moisture content (Binley et al., 2002), biodegradation of hydrocarbons (Atekwana et al., 2000), salt tracer experiments (Kemna et al., 2002 ; Robert et al., 2012) and heat injection experiments (Hermans et al., 2012b). It was also used in the characterization of geological structures, for example in the exploration of geothermal systems, where hydrothermal fluids may generate high contrasts of resistivity (Pérez-Flores and Gomez Trevino, 1997; Bruno et al., 2000; Garg et al., 2007; Arango-Galván et al., 2011).

Besides the characterization of shallow geothermal systems themselves, their impact on the groundwater temperatures in the aquifer may be important since their exploitation yields cold and heat plumes (Molson et al., 1992; Palmer et al., 1992 ; Warner and Algan, 1984) which may influence aquifer properties and groundwater chemistry (e.g. Jesuβek et al., 2013) and microbiology (Brielmann et al., 2009). Haehnlein et al. (2010) pointed out that, if laws and rules exist in some countries to limit the temperature difference caused by the use of geothermal systems, the development of anomalies is rarely monitored. With the growth of the demand for renewable energy, we can expect that regulations will become stricter and controls of installations more common. New monitoring technologies will be needed and ERT may play an important role to monitor spatially, i.e. not only in wells, the variations of temperature in the aquifer. For example, the temperature changes observed on operating GWHP systems (e.g. Vanhoudt et al., 2011) are typically in the range of temperature that could be detected by ERT.

ERT aims at imaging the electrical resistivity distribution of the subsurface. Using petrophysical relationships such as Archie's law, one may recover indirect parameters such as saturation, water electrical conductivity or total dissolved solid content. Bulk electrical resistivity also decreases with temperature (e.g. Revil et al., 1998). In most studies, temperature effects are undesirable and may create artifacts in the interpretation, a correction term is applied to remove the influence of temperature variations (Hayley et al., 2007; Sherrod et al., 2012). Few studies used time-lapse ERT to monitor directly temperature changes (Ramirez et al., 1993 ; Labrecque et al., 1996b), generally in a context quite different from GWHP or GSHP systems.

Hermans et al. (2012b) monitored with time-lapse surface ERT a heat injection experiment at a relatively small scale (45 m) and at shallow depth (2 to 4.5 m). Their results show that ERT is a reliable tool to monitor temperature changes and may be a method of choice for the design and the monitoring of geothermal systems. However, the results need to be extended to deeper and more complex, heterogeneous reservoirs, as it will be considered in this paper. ERT-derived temperatures were very close to temperatures modeled using a calibrated coupled groundwater and heat flow and transport model bringing additional constraints on the thermal properties of the aquifer.

For deeper reservoirs, the rapid decrease in resolution and sensitivity of surface ERT becomes a major drawback (Caterina et al., 2013). It is then necessary to consider borehole ERT to improve resolution (Perri et al., 2012). For example, Prevedel et al. (2009) installed deep (600 to 750 m) borehole electrodes to monitor the migration of CO_2 within a storage reservoir (Bergmann et al., 2012). For cross-hole ERT, the results obtained for a specific study are more easily extendable than for surface ERT because resolution patterns are not depth dependent.

In borehole ERT, electrodes are located under the ground surface, either fixed at the outer-edge of the casing or mounted on cables with the borehole fluid ensuring the electrical contact with the surrounding rock. In the latter case, borehole fluid is generally more conductive than the rock and may influence resistance measurements (Doetsch et al., 2010). Using time-lapse ERT, the relative fluid effect will be almost similar at each time-step and should be insignificant in inversion results (Nimmer et al., 2008).

In this paper, we study the ability of ERT to monitor temperature changes in a heterogeneous aquifer and follow thermal tracing experiments. We pumped water from a gravel aquifer, heated it and reinjected it in a second well, similar to a GWHP system operation.

The paper is organized as follows: first, the field site is described; second, the methodology is presented; then, the results of the ERT monitoring are compared with direct measurements in wells; finally, conclusions are presented.

2. Field Site

The study site is located in Hermalle-sous-Argenteau in Belgium near the Belgian-Dutch border (Figure 1). It lies on the alluvial aquifer of the Meuse River. A pumping well and 8 piezometers were already present on the site since the 1980's and 11 new piezometers were drilled in June 2012 together with an injection well. They were arranged in three different panels crossing the main flow direction between the injection well and the pumping well in order to study the spatial variability during tracing experiments (Pz10 to 20, Figure 2).

Borehole logs enabled to divide the deposits in four different units. The first layer consists of loam and clay with a thickness between 1 and 1.5m. The second layer is composed of gravel in a clayey matrix. The bottom of this layer is found at depth between 2 and 3.2m. These two first layers have little importance in this study because they are located in the unsaturated zone. The water table lies at approximately 3.2m depth, with a very small gradient towards the northeast which is the main direction of flow (Figure 2). The third unit is composed of gravel and pebbles in a sandy matrix. The quantity of sand decreases with depth, whereas the size of the pebbles increases with depth, a vertical variability is thus present. Lateral variability in the grain size distribution of the deposits is also expected in this heterogeneous aquifer, leading to variable hydrogeological parameters. Between 9.7 and 10.1 m, the Carboniferous bedrock composed of folded shales and sandstones is found.

In the middle panel, the outer piezometers are screened on the whole thickness of the alluvial aquifer. This is also the case for the injection and pumping wells. Except for the latter, they were equipped with a distributed temperature sensing (DTS) system to monitor the temperature during the experiment (Leaf et al., 2012 and references therein) with a spatial resolution of 0.5m. Pz14 and Pz16 were screened at two different levels, with a 2m long screen between 4 and 6m depth and 1m screen between 8.5 and 9.5m. All other piezometers were screened at two different levels, with a 1m screen between 4.5 and 5.5m depth and a 2m screen between 8 and 10m depth. In the middle of each screened zone, a groundwater temperature logger was placed to monitor the temperature and the pressure during all the experiment.

Previous studies have shown that the gravel aquifer is very permeable. Calibrated hydraulic conductivity values were found previously between 1.2 10^{-1} and 2 10^{-3} m/s (Dassargues, 1997; Derouane & Dassargues, 1998; Brouyère, 2001). With such values, it is possible to inject at a rate much higher than Hermans et al. (2012b) who were limited by the low hydraulic conductivity of fine sands and the small thickness of the aquifer.

3. Methodology

3.1. Heating and injection procedure

The experiment consists of an injection and pumping test. The groundwater is pumped from the pumping well, located in the northeastern part of the site, downstream from the injection well. We used a pumping rate of 30 m³/h. Given the high hydraulic conductivity values of the aquifer, the corresponding drawdown is only 5 cm in the pumping well and 4 cm in Pz19 (5 m upgradient from the well). The pumping process ensures that the main direction of flow will cross the three intermediate panels. Pumping was started one day before the beginning of the injection of heated water, far early enough to reach a steady-state flow, and continued after the end of injection.

We used a mobile water heater (AQUAMOBIL DH6 system) to heat the water injected in the aquifer. It can work at a maximum rate of 3 m³/h with a difference in temperature of about 30°C. Given the high hydraulic conductivity of the aquifer, we decided to inject at this maximal rate. During the injection phase, 3 m³/h of the pumped water were derived in a stocking tank, passed through the water heater and injected in the injection well. The mean temperature of the extracted water at the time of the experiment (October-November 2012) was 13°C. With the maximum injection rate, the temperature of the injected water reached a stabilized mean value of 38°C.

Injection started on October 30th and lasted for 1 day, resulting in the injection of 72 m³ of heated water. Using groundwater also for injection, the transformation of ERT results into temperatures will be direct and only require a unique petrophysical relationship. However, the heterogeneity of the aquifer and the advection component make the experimental set-up quite complex.

3.2. Petrophysical relationship linking temperature and conductivity

The aim of the petrophysical relationships is to quantify the link between bulk electrical conductivity and temperature. Bulk electrical conductivity is generally expressed as a function of porosity, grain size and tortuosity (often joined in a term called formation factor), saturation, fluid electrical conductivity and surface conductivity. In this case, we are interested in the saturated zone (saturation = 1) where the grain size distribution is dominated by gravel with very few fine elements. We can thus neglect the surface conductivity which is very low for coarse grains (Revil and Linde, 2006). With this assumption, the link between bulk electrical conductivity σ_b and fluid electrical conductivity σ_f is

$$\sigma_b = \frac{\sigma_f}{F} \qquad (1)$$

where F is the formation factor (Archie, 1942). The latter is variable spatially, depending on the lithology. In the case of a monitoring study, we measure bulk electrical resistivity at different time steps and compare it to a reference state, called the background. If we take the ratio of equation 1 between a specific time-step, representing state 2, and the reference background, representing state 1, we have

$$\frac{\sigma_{b2}}{\sigma_{b1}} = \frac{\sigma_{f2}}{\sigma_{f1}} \qquad (2)$$

and the relation is not dependent on the formation factor anymore. In equation 2, σ_{b1} and σ_{b2} are determined with ERT after inversion of resistance data and σ_{f1} is either measured on the field directly or deduced from the temperature of the formation water in the aquifer. The only unknown in equation 2 is the fluid electrical conductivity at state 2, which can be expressed as

$$\sigma_{f2} = \frac{\sigma_{b2}}{\sigma_{b1}} \sigma_{f1} \qquad (3)$$

Through equations 1 to 3, we see that the variation in bulk electrical conductivity in the saturated zone is related to a variation of the fluid electrical conductivity only. The latter can be caused by a change in fluid salinity or by a change in temperature. If we assume that the salinity of the fluid remains constant during the experiment, the water electrical conductivity depends only on temperature.

Hermans et al. (2012a) have shown that for long term experiments (storage phase) at relatively high temperature, the link between temperature and electrical resistivity may be more complex, due to precipitation/dissolution effects related to temperature changes, as shown by Robert et al. (2013). However, in this case, the temperature difference is about 25°C and should rapidly decrease due to dispersion effects. The variation of salinity with changing chemical equilibrium should be relatively small. If this effect is not negligible, an additional term in equation 5 should be added and calibrated to derive temperatures.

In the temperature interval considered in this experiment (10 to 40°C globally, and 10 to 20°C for the panel monitored with ERT), a linear dependence can be assumed between temperature and fluid electrical conductivity (e.g. Sen and Goode 1992 and Hayley et al. 2007 or Hermans et al. 2012b for applications). This relation can be expressed as

$$\frac{\sigma_{f,T}}{\sigma_{f,25}} = m_f (T - 25) + 1 \qquad (4)$$

where $\sigma_{f,T}$ is water electrical conductivity at temperature T in °C, $\sigma_{f,25}$ is the conductivity at 25°C, considered as the reference temperature (another reference could be chosen as well) and m_f is the fractional change in electrical conductivity per degree Celsius at the reference temperature.

A water sample was taken on the site and relation 4 was verified experimentally in the laboratory (Figure 3). Figure 3 shows the results up to 20°C (temperature encountered in the middle panel), but the trends remains the same until 40°C. Fitting a linear curve to the experimental points, we found m_f equal to 0.0194 and the conductivity at the reference temperature (25°C) is equal to 0.0791 S/m. The value for the fractional change per degree Celsius is in the same range as observed by Hayley et al. (2007) and Hermans et al. (2012b).

Introducing equation 4 into equation 3, we can express the temperature T (in °C) according to bulk electrical conductivity, water electrical conductivity at the temperature of reference and at the temperature of the background and the fractional change per degree Celsius

$$T = \frac{1}{m_f}\left[\frac{\sigma_{b2,T}}{\sigma_{b1}}\frac{\sigma_{f1}}{\sigma_{f,25}} - 1\right] + 25 \quad (5)$$

where $\sigma_{b2,T}$ represents the bulk electrical conductivity at the time-step for which we try to determine the temperature.

3.3. Electrical resistivity measurements

The two outer piezometers of the middle panel (Pz13 and Pz17 on Figure 2) were equipped with borehole electrode cables with 0.5m spacing. Each borehole has thus 13 electrodes made of stainless steel located from 3.5 to 9.5 m depth. The first electrode is located just below the water table whereas the last electrode is located just above the bedrock.

The two boreholes are separated horizontally by 4.5 m. The thickness covered by the electrodes is 6 m. The aspect ratio, i.e. the ratio of the separation between boreholes and the length of the equipped borehole is thus equal to 0.75. This value is often considered as the maximum acceptable value to obtain a sufficient resolution. Optimal resolution is generally achieved with an aspect ratio of 0.5 (LaBrecque et al., 1996b).

We used a combination of bipole-bipole (also called AM-BN) and dipole-dipole (AB-MN) configurations as measuring sequence. The first one has a better signal-to-noise, but a lower resolution (Zhou and Greenhalgh, 2000). For bipole-bipole measurements, we measured every possible configuration. For the dipole-dipole, we kept only the cross-borehole measurements, using a dipole spacing ranging from 0.5 to 5m and measuring dipoles sharing one electrode. The complete data set contains 969 possible measurements.

We used an ABEM Terrameter LS to acquire the data with an acquisition delay of 0.5s and an acquisition time of 1s. We used a standard deviation limit of 1% on the repeatability error after 3 stacks to filter the data. For almost each time step, we collected both normal and reciprocal measurements to assess the error level on the data. The latter are obtained by swapping current and potential electrodes (LaBrecque et al., 1996a). Acquiring a complete data set took about 45 minutes (normal and reciprocal measurements).

The error level was estimated using both the methods of Slater et al. (2000) and Koestel et al. (2008). They both used the reciprocal error to derive a linear relationship between the mean measured resistance R_m (mean between normal and reciprocal resistance, in Ohm) and error e (in Ohm) defined as the difference between normal and reciprocal measurements

$$|e| = a + bR_m \quad (6)$$

where a is an absolute error (Ohm) and b is a relative error. Slater et al. (2000) considered the envelope curve as error model, which can be considered as conservative, since the mean error is overestimated. Koestel et al. (2008) worked with standard deviation of logarithmic bins to determine the coefficients. This method may result in a mean error model, less conservative.

Nguyen et al. (2011) have shown that the noise level characterization is of great importance in time-lapse studies and should always be investigated carefully. If the noise levels are too different between time-steps, it may prevent a quantitative interpretation of monitoring data. If noise levels are almost similar, one should choose a common error model to invert all data sets. We calculated error models for both methods and each time-step. We chose a common error model with an absolute error of 0.002 Ohm and a relative error of 0.5%. We tested different error level around these values, with few differences in the final images, both qualitatively and quantitatively.

The aim of cross-hole electrical resistivity was to detect the first arrival of the tracer, the maximum temperature reached in the middle panel and, to image vertical and lateral variations in the temperature distribution. Data sets were collected about every six hours during the injection and the day after. For the next days, we increased the time-steps to about 18h, with one or two sections per day. The total monitoring time was 6 days, time at which the resistivity distribution had almost returned to the background distribution. For comparison, a DTS system was set in both boreholes to control the temperature directly and assess the ability of ERT to derive reliable temperatures.

3.4. Inversion procedure

In electrical resistivity tomography, the solution of the inverse problem is non-unique. A common way to solve such inverse problems is to add a regularization constraint to the least-square problem (Tikhonov and Arsenin, 1977). The problem is then to minimize, through an iterative process an objective function of the form

$$\psi(\mathbf{m}) = \left\|\mathbf{W}_{\mathbf{d}}(\mathbf{d} - \mathrm{f}(\mathbf{m}))\right\|^2 + \lambda \left\|\mathbf{W}_{\mathbf{m}}\mathbf{m}\right\|^2 \qquad (7)$$

where λ balances between the data misfit (first term of the right hand side of equation 7) and the model a priori characteristic (second term), **d** represents the vector containing the data, expressed as the logarithm of measured impedance, **m** is the model of the logarithm of subsurface electrical conductivity, f(**m**) is the forward operator, $\mathbf{W_d}$ is the data weighting matrix using the reciprocal error as estimate (equation 6) and $\mathbf{W_m}$ is a matrix describing an a priori characteristic of the conductivity model. Several forms are possible for $\mathbf{W_m}$, for example to include prior information (e.g. Hermans et al. 2014). The most common method, used in this study, is to penalize roughness to describe smooth model variations (deGroot-Hedlin and Constable, 1990).

With time-lapse data sets, we are more interested in the change in electrical conductivity than in the absolute value of conductivity. Generally, the process of inversion is adapted in order to improve inversion results. In this paper, we do not consider coupled inversion of time-lapse ERT data and hydrogeological models (e.g. Irving and Singha 2010). Three main procedures, with several variants, exist to invert for time-lapse ERT data (e.g. Miller et al. 2008), namely independent inversion, time-constrained or reference model inversion and difference inversion. In the first one, inversion results obtained separately are simply substracted, which should eliminate systematic errors but amplify uncertainties in the data. For temporally constrained schemes, a regularization operator is added in the time dimension in addition to the space dimensions, to minimize changes between successive sections (e.g. Karaoulis et al., 2011, 2014). This enables 4D inversions of ERT time-lapse data sets and has already shown to be efficient in tracer tests (Revil et al., 2013). In this study, we used the difference inversion scheme (Kemna et al., 2002) where the problem is formulated in terms of variations for both data and model. Equation 7 becomes

$$\psi(\mathbf{m}) = \left\| \mathbf{W}_{\mathbf{d}} (\mathbf{d} - \mathbf{d}_0 + \mathrm{f}(\mathbf{m}_0) - \mathrm{f}(\mathbf{m})) \right\|^2 + \lambda \left\| \mathbf{W}_{\mathbf{m}} (\mathbf{m} - \mathbf{m}_0) \right\|^2 \quad (8)$$

where $\mathbf{d}_0$ and $\mathbf{m}_0$ are respectively the data set and the model corresponding to the background state. The results obtained for the background are thus used as reference for subsequent inversions. This method should reduce the systematic error and provide a faster convergence. (LaBrecque and Yang, 2000).

To compare the successive models in the monitoring study, it is important that all data sets are inverted with the same level of data misfit corresponding to the expected noise level. Indeed, over-fitting the data may create artifacts of inversion in the corresponding image, whereas the contrary would results in an over-smoothed inverted section (LaBrecque et al., 1996a). To achieve this, the iteration process is stopped when the root-mean-square (RMS) value of error-weighted data misfit

$$\varepsilon_{\mathrm{RMS}} = \sqrt{\frac{\left\|\mathbf{W}_{\mathbf{d}}(\mathbf{d} - \mathrm{f}(\mathbf{m}))\right\|^2}{\mathrm{N}}} \qquad (9)$$

with N representing the number of data, reaches the value 1 for a maximum possible value of λ, corresponding to data fitted to its error level. At each iteration, λ is optimized to obtain the minimum value of $\varepsilon_{\mathrm{RMS}}$. When, $\varepsilon_{\mathrm{RMS}}$ is inferior to 1, we looked for the unique value of λ that satisfies the data misfit criterion ($\varepsilon_{\mathrm{RMS}} = 1$).

We used the code CRTomo (Kemna, 2000) to invert our data. This code is a 2.5D inversion code; it means that the electrical conductivity distribution is assumed to be constant in the direction perpendicular to the section and that the effect of boreholes themselves cannot be taken into account (Nimmer et al., 2008; Doetsch et al., 2010). Effects caused by boreholes are of more concern when the investigated site is located in high resistive rocks. They may also be, at least partly, avoided with time-lapse inversion. Indeed, we can expect that, if present, 3D artifacts will be compensated because present in both background and monitoring states (Nimmer et al., 2008). However, a possible 3D effect when imaging a contrasting plume, also called shadow effect, is that the plume is imaged even if it is outside the image plane, because the 3D heterogeneity caused by the moving tracer is not taken into account in the 2.5D inversion scheme (Nimmer et al., 2008). This may result in bias in the breakthrough curve, leading to an apparent more diffuse behavior of tracers (Vandenborght et al., 2005).

We used a grid with square elements of 0.25 m x 0.25 m, to have two elements between electrodes, extended laterally and in depth for inversion. ERT-borehole 1 is located at abscissa 1 m and ERT-borehole 2 at abscissa 5.5 m on the grid.

To assess the quality of the ERT image, we used the error weighted cumulative sensitivity matrix (Kemna, 2000; Caterina et al., 2013). The cumulative sensitivity **S** is defined as

$$\mathbf{S} = \mathrm{diag}(\mathbf{J}^{T}\mathbf{W}_{d}^{T}\mathbf{W}_{d}\mathbf{J}) \quad (10)$$

where **J** is the Jacobian matrix and T denotes the transpose operator. **S** depends on both the distribution of resistivity in the model parameters and the data weighting matrix which depends on the error assessment. A high value of sensitivity for a parameter signifies that a change of its resistivity would strongly influence the data. In contrast, a low value of sensitivity is characteristic of a parameter having less influence on the predicted data. Such a low sensitivity zone will most likely be badly resolved in the inverted section. However, it has to be noted that high sensitivity does not necessarily mean high resolution.

4. Results and discussion

4.1. Cross-borehole ERT background

The background image was obtained using equation 7, corresponding to the smoothness-constrained solution (Figure 4). In the zone between the boreholes, we see that the resistivity lies between 100 and 200 Ohm-m, with lower resistivities at the bottom of the section. These resistivity values are characteristic of saturated sand and gravel. The lower resistivity observed at the bottom of the aquifer corresponds with coarser gravel and a lower sand content.

The resistivity tends to increase towards the unsaturated zone (above – 3.5m), but there was no electrode in this part of the section (the electrode at – 3 m was modeled but not used for any configuration). However, we do not expect these absolute values to be accurate due to borehole and 3D effects in the inversion (Nimmer et al., 2008).

The sensitivity pattern is typical of cross-borehole measurements (Figure 5). The sensitivity is high in the neighborhood of the boreholes and decreases towards the middle part of the section. The sensitivity is lower in two opposite triangles in the upper and bottom part of the saturated zone, due to a smaller coverage of data points in this zone. The lowest sensitivity values are found in the unsaturated zone. The electrical contact through borehole electrodes was not possible because the borehole is not filled with water in this part; no surface electrodes were used to improve the resolution, because the aim is to image temperature changes in the saturated zone. Given the sensitivity values and the aspect ratio, we assume that the chosen configuration is sufficient to monitor temperature changes within the section.

4.2. Cross-borehole ERT monitoring results

Before looking at inverted data, it is important to qualitatively check if the acquired data contains some information about the monitored process. We calculated the mean resistance of each data set after removing data with repeatability error higher than 1% (870 points remaining). The mean resistance for the background data set is 14.31 Ohm. The first monitoring set was taken after 7h of injection, the mean resistance slightly increases, but not significantly (Figure 6). This is likely an effect of noise on the data. We can state that temperature changes are too small to influence the measured resistance. The same effect can be observed on individual measurements. The mean resistance then decreases with time to reach a minimum value of 13.76 Ohm after 30 to 35 hours after the beginning of injection, which corresponds to 6 to 11 hours after the end of injection. After the minimum, the mean resistance starts to increase and slightly tends to its initial state, even if it is not totally reached at the end of the monitoring process.

Figure 6 can be seen as a qualitative mean breakthrough curve of the heat tracing experiment. It enables to derive two important parameters: the first detected arrival of heat, which occurs between 7 and 12 hours, and the maximum changes, which occurs between 30 and 35 hours. The time-lapse data sets were inverted using equation 8, i.e. the results of Figure 4 are used as a reference and we inverted data differences to derive model perturbations. We kept the same error model for all inversions and we reached a value of ε_{RMS} equal to 1 for all inversions, ensuring that all models are fitted to the same level of noise. The results are presented as percentage change of resistivity

$$\Delta\rho = \frac{\rho_{\mathrm{i}} - \rho_{\mathrm{BG}}}{\rho_{\mathrm{BG}}} \times 100 \quad (11)$$

where ρ_{i} is the resistivity of the time-lapse section and ρ_{BG} is the resistivity of the background section. A negative value corresponds to a decrease in resistivity (or increase of conductivity) and a positive value corresponds to an increase in resistivity.

Given the process that is monitored, only negative changes related to an increase in temperature are expected. However, in the inverted time-lapse sections (Figure 7) positive changes of resistivity appear. They are limited in absolute value to +5% in the unsaturated zone which suffers from a very poor resolution, and +3% in the saturated zone. We relate these positive changes to the propagation of data noise in the inversion process (Robert et al. 2012). Consequently, we consider that variations in the range -3% to +3% cannot be directly related to temperature variations. They are whitened in the figure. If -3% is the minimum change in resistivity that can be correctly imaged, the limit of detection of ERT for temperature at 13°C for temperature is about 1.2°C (equation 5).

The inverted time-lapse sections (Figure 7) show a general behavior of the plume similar to the one observed from the mean resistance. After 7h (not shown), changes in resistance are low and under the level of noise, yielding a section with no changes, i.e. the background model is sufficient to explain the data. After 12h, changes of resistivity about - 5% appear. Then, the decrease in resistivity becomes stronger and reaches a maximum between 25 and 35 h. Afterwards, the contrast becomes less strong and after 90 h, almost all changes are below 5%. It signifies that their level becomes low to be interpreted quantitatively (close to the limit of detection). However, their spatial distribution is coherent with previous time steps, so it means that the aquifer has not returned to its initial state yet, which is confirmed by the mean resistance.

The apparent decrease in resistivity observed in the 101 h section is likely due to an artifact of inversion since it is not physically plausible and does not appear in any other sections. The fact that all other anomalies observed in the sections are recurrent for all time steps and that their amplitude variation follows the trend of classical breakthrough curves validate qualitatively the results of inversion. If some anomalies were related to artifacts of inversion, they would be more randomly distributed for the different time-steps.

The advantage of crosshole ERT compared to direct measurements is to provide a spatial distribution of the changes occurring in the aquifer. Figure 7 clearly shows that the changes in resistivity are not homogeneously distributed in the aquifer. Most important changes are observed below -7.5 m depth. This part of the alluvial aquifer is dominated by very coarse gravel with pebbles and a limited amount of sandy matrix, as was observed during drilling. The hydraulic conductivity of the bottom part is higher and the flux is greater, so a major part of heat is flowing in this zone of the aquifer. In the upper part, the convection velocity is slow and the maximum change in temperature is much lower, below the minimum change that ERT can detect. Laterally, we also see variations. The maximum change does not occur in the middle of the section, along the supposed main flow direction. It is located closer to ERT-borehole 1. The resistivity changes are smaller in the middle part, whereas there are a little bit higher in the neighborhood of ERT-borehole 2. Since sensitivity is smaller in the middle section, there is more uncertainty related to those parameters. However, this trend will be confirmed by direct measurements in boreholes (section 4.4).

The lateral variations observed in the ERT sections suggest a degree of heterogeneity that was not clearly distinguishable on borehole logs. Zones of preferential flows modify the expected flow direction and result in sections showing a complex spatial behavior. We will see later that these observations are confirmed by direct measurements in borehole.

4.3. ERT-derived temperatures

For simplicity, we decided to use a constant value of σ_{f1} (equation 5) to transform the ERT images into temperature sections.

Equation 4 proposes a linear relationship between water electrical conductivity and temperature. We thus deduce σ_{f1} based on our direct measurements of temperature. Theyshow that the temperature profile is not constant everywhere in the aquifer and in the ERT section (Figure 8). In ERT-borehole 1, a maximum temperature difference of 1.3°C is observed between the top and the bottom of the aquifer. It is slightly less in ERT-borehole 2. The mean temperature in the two boreholes is also different: 12.8 °C in ERT-borehole 1 (Pz13) and 13.6°C in ERT-borehole 2 (Pz17). We took the mean temperature of both ERT-boreholes (13.2°C) and derived with equation 4 a water electrical conductivity of 0.061 S/m. Another solution would have been to interpolate temperatures between boreholes, but it would have made the process more complex without ensuring an improvement of the results.

This process has two additional assumptions. First, the specific electrical conductivity of water is constant with time. This was controlled using water samples collected in Pz15 during the test. The changes in the specific conductivity of water are smaller than 1%. The increase in temperature does not seem to favor precipitation or dissolution of minerals. The second assumption is that, at a given temperature, the ratio $\sigma_{f1}/\ \sigma_{f,25}$ (equation 5) is constant in space, or similarly that m_f is constant in the whole section. Indeed, if the specific conductivity of water varies in the section, the conductivity at a given temperature varies in the same proportion and the influence on the calculation of temperature is limited. Given the values generally observed in the literature, this assumption is not too severe.

The spatial distribution of temperature (Figure 9) is similar to electrical resistivity changes (Figure 7). Maximum changes of temperature are observed in the neighborhood of ERT-borehole 1, with a maximum temperature of 21°C, which corresponds to an increase around 8°C. However, we know that the background temperature in ERT-borehole 1 is slightly below the mean value chosen to draw these sections. Considering the limit of detection of 1.2°C at 13°C, temperatures in the range 13.2-14.4°C are only indicative of a small raise in temperature, but the exact value cannot be derived. In addition, we have an error related to the mean water electrical conductivity used in equation 5.

4.4. Comparison with direct measurements

The layout of the study site enabled to make a lot of direct measurements in piezometers, at different levels in the aquifer. To compare with ERT results, we have DTS measurements in ERT-boreholes 1 and 2, and groundwater temperature loggers at two levels in the three intermediate piezometers Pz14 to Pz16.

The quicker arrival of heat in the bottom part of the aquifer (figures 7 and 9) is confirmed in intermediate piezometers (Figure 10 for Pz15). In the upper part, the arrival is very slow and a clear increase in temperature is only visible after 2 days. The oscillations in the signal are disturbances due to sampling of water by pumping from the piezometer. The amplitude of the signal remains very small, below 1°C at the end of the test. Actually, the peak would only be observed after 10 days with an amplitude of about 1.15°C. The same is observed in Pz16 (1°C after 10 days). In Pz14, the change is slightly higher (2°C after 4 days). In the bottom part, the arrival of heat is quicker, after a few hours, with a range of temperature slightly above the limit of detection of ERT. This is totally in agreement with the ERT sections. Spatially, the temperatures observed with ERT are also coherent with direct measurements. The temperatures observed in the bottom part of Pz14 to 16 have a decreasing trend from Pz14 to Pz16, which is also evident from ERT sections where the zone near ERT-borehole 1 is hotter than the middle of the section. As an example, the maximum ΔT in Pz14 is 4.2°C, whereas it is only 2.9°C in Pz15. We can conclude that the qualitative observations on the spatial and temporal distribution of temperature are confirmed by direct measurements.

To verify the ability of ERT measurements to quantify temperature, we rely on two different indicators. First, we can draw breakthrough curves at the locations of groundwater temperature loggers to compare the direct measured curve with the ERT-derived curve. This will give insights on the ability to quantify temporally temperature changes. Secondly, we may compare temperature logs at ERT-borehole 1 and 2, to investigate quantitatively the spatial distribution of temperature.

Figure 11 shows the breakthrough curves in the bottom part of Pz14 (A) and Pz15 (B) for both direct measurements and ERT. We used the temperatures measured in the corresponding boreholes to determine σ_{f1} in equation 5. For both piezometers, ERT does not detect directly that heat is arrived, because the changes are small, below the sensitivity of the method. However, the rising part of the curve is well resolved with an ERT-derived temperature almost exactly the same as measured directly. The maximum is overestimated, with an error of about 0.5°C in Pz14. The maximum change being 4°C, it represents an error of about 12.5%. In Pz15, the fit is less good, but the maximum change is lower and the spatial smoothing of the inversion process may yield an overestimation of the temperature. For both cases, the tail of the curve is overestimated by ERT-derived temperatures. This effect would lead to an overestimation of the thermal dispersivity of the aquifer if ERT results were used alone. This could be related to a 3D effect (shadow effect), because the maximum of the plume, even if not in the section anymore, is still influencing measurements.

It must also be kept in mind that the volume investigated by ERT and direct measurements is not the same. Groundwater temperature loggers give a very local measurement inside the piezometer which is itself a singularity inside the aquifer. ERT inversion results give a mean resistivity over the surface of the corresponding cell (here 0.25 cm x 0.25 cm). Another possibility would be an increase of the specific conductivity of formation water due to dissolution of minerals related to the increase of temperature. However, given the quick decrease of temperature when we move away from the injection well, this effect is negligible. This is confirmed by the samples collected in Pz15 which shows an almost constant specific conductivity.

Temporally, the results are very satisfactory because the raising part, the maximum and the tailing of the curve are imaged at correct times. In this specific case, the time resolution of ERT is only of a few hours. It signifies that we cannot expect to detect the first arrival with precision. Given the material used, we could achieve a time resolution of half an hour, by reducing acquisition time and acquisition delay which were chosen conservative.

The comparison of ERT-derived temperatures with DTS measurement in the two ERT-boreholes yields contrasted results and conclusions (Figure 12). In contrast with figure 9, where we used a constant value of σ_{f1}, the temperatures measured with the DTS for the background profile were here used to derive a specific value of σ_{f1} for each depth level. In addition, DTS measurements were averaged on the time interval corresponding to the duration of a complete ERT data acquisition. Consequently, the match would be perfect if we would derive temperatures for the background ERT profile using equation 5.

In ERT-borehole 1 (Figure 12A), ERT results show the same behavior as observed in Figure 7, with higher temperatures in the bottom part of the aquifer, and smaller in the upper part. In contrast, DTS measurements yield an almost constant temperature on the whole thickness of the aquifer. This is a quite surprising observation, because all direct measurements made on the site have shown a clear contrast in temperature distribution between the bottom and upper parts of the aquifer. We think that DTS measurements are influenced by specific borehole conditions and do not reflect the true formation temperature. A possible explanation is that the water suffers from some mixing in and around the well.. ERT measurements, even if influenced by the borehole fluid, are sensitive to the variations outside the borehole itself. This effect may also explain why temperature near ERT-borehole 1 seems to be higher in Figure 9 in the upper part of the aquifer whereas it is not the case in the middle part of the section.

In ERT-borehole 2 (Figure 12 B, C and D), the agreement between ERT-derived temperatures and DTS logs is better. It confirms that the hot spot observed near this borehole in Figure 9 is not an artifact of inversion but is related to an increase in temperature. Globally, DTS measurements show slightly less contrast than ERT, maybe also due to borehole conditions as observed in ERT-borehole 1. Quantitatively, ERT-derived temperatures are close to DTS temperatures for the rising and maximum part of the breakthrough curve (Figure 12 B and C), but suffer from an overestimation for the tail (Figure 12 D), as it was observed in Figure 11. Such an effect would be reduced in a storage experiment with conditions of no flow.

The comparison of ERT results with direct measurements and their good agreement confirm that the alluvial aquifer is heterogeneous and complex. Instead of a unique heat plume in the middle part of the section, we observed two separated arrivals with a minimum temperature observed in the middle.

5. Conclusion

The growing demand for renewable energy leads to an increase in the development of geothermal energy projects. Heat storage has become a common energy storage technology and heat is a common tracer in hydrology and hydrogeology. The variation of electrical resistivity/conductivity of water, soils and rocks is a well-known phenomenon and has been studied for several decades. However, the potential of ERT, a method mapping the electrical resistivity of the subsurface, to monitor and quantify temperature was barely approached in the literature.

In this paper, we investigated the ability of crosshole ERT to monitor a heat tracing experiment in a complex heterogeneous alluvial aquifer. The studied section was located perpendicular to the main direction of flow to cross the plume of heated water. The results, corroborated by direct measurements in several control piezometers, highlight the ability of ERT to qualitatively monitor the variations of temperature in the aquifer. Spatially, it enabled to map the horizontal and vertical extent of the plume, as well as the zones of maximum temperatures, what would not be feasible with costly and limited direct measurements.

If information on the initial fluid conductivity is available, ERT results may be interpreted quantitatively in terms of temperature. The temperatures estimated from ERT were relatively close the ones observed directly during the rise and maximum part of the curve. An overestimation, likely related to 3D effects, was observed for the tail of the breakthrough curve. The error made can be estimated to be between 10 to 20 %, which is a fair value for indirect measurements. The precision of the method may be better in more favorable cases, for example in no or low flow conditions. 3D imaging procedure using more than two wells should also improve the reliability of electrical resistivity monitoring results, yielding a better characterization of temperature distribution.

The limit of quantification of temperature changes depends on the noise level observed on the site. ERT requires for an error assessment in order to avoid artifacts in the inverted sections. The higher the noise level, the lower the resolution of ERT to derive temperature changes. In this case, we observed after inversion positive changes of electrical resistivity up to 3% in the saturated zone. Those changes were not physically related to the tracing experiments and enabled us to estimate a limit of quantification for ERT around 1.2°C for temperature changes.

In contrast with surface ERT, the resolution of crosshole ERT is not depth-dependent but depends mostly on the aspect ratio, the electrode spacing and the distance to the boreholes. In this case, we achieve an aspect ratio of 0.75 with 13 electrodes. A greater distance between boreholes would require a greater electrode spacing or the use of more electrodes. Standard measurement devices generally accept 24 to 32 electrodes per borehole. Considering an electrode spacing $a=0.5\ m$, we successfully imaged a heterogeneous heat plume with a thickness about $5a$ and a width of about $4a$. The results obtained in this study could be easily extended to other experiment keeping similar parameters. The resolution could even be refined using better aspect ratio or more electrodes. The scale of this experiment could be applied for the control of aquifer thermal energy storage (ATES) located in alluvial plains. For deeper and larger systems, it would require larger distances between electrodes and boreholes or the use of set-up with more than two boreholes.

In this experiment, we only achieve a time resolution of a few hours. Our measuring procedure takes about 45 minutes. However, it is possible to reduce acquisition delay and acquisition time of each measurement. It would allow to achieve a time resolution of less than 30 minutes. Avoiding the complete collection of reciprocal at each time step would further divide the time to collect the data by two.

The results presented in this paper suggest that ERT should be considered when designing heat tracing experiments to derive the parameters governing heat flow and transport in the subsurface or geothermal systems. It should also be used to assess the complexity of the concerned reservoirs. It also appears that ERT could be a useful tool to monitor and control geothermal systems once they are in operation. A proper configuration of ERT wells, depending on the installed configuration, should enable to control the temperature distribution in the reservoir. This may be of crucial importance to better describe the thermal affected zone or assess the possible influence of the system on groundwater chemistry or microbiology.

Acknowledgement

We would like to thank the associate editor and two anonymous reviewers for their pertinent comments and suggestions which have helped to improve the manuscript. We also thank the F.R.S.-FNRS and the « Fondation Roi Baudouin – Ernest Dubois Award » for their financial support during the PhD of Thomas Hermans.

References

Allen, A., Milenic, D., 2003. Low-enthalpy geothermal energy resources from groundwater in fluvioglacial gravels of buried valleys. Applied Energy, 74, 9-19.

Arango-Galván, C., Prol-Ledesma, R.M. , Flores-Márquez, E.L., Canet, C., Villanueva Estrada, R.E., 2011. Shallow submarine and subaerial, low-enthalpy hydrothermal manifestations on Punta Banda, Baja California, Mexico: geophysical and geochemical characterization. Geothermics, 40, 102-111.

Archie, G. E., 1942. The electrical resistivity log as an aid in determining some reservoir characteristics. Transactions AIME, 146, 54-62.

Atekwana, E.A., Sauck, W.A., Werkema, D.D., 2000, Investigations of geoelectrical signatures at a hydrocarbon contaminated site, Journal of applied geophysics, 44, 167-180.

Anderson, M.P., 2005. Heat as a ground water tracer. Ground Water, 43, 951-968.

Bergmann, P., Schmidt-Hattenberger, C., Kiessling, D., Rücker, C., Labitzke, T., Henninges, J., Baumann, G., Schütt, H. 2012 Surface-downhole electrical resistivity tomography applied to monitoring of CO_2 storage at Ketzin, Germany. Geophysics 77, B253-B267.

Binley, A., Winship, P., West, L.J., Pokar, M., Middleton, R., 2002. Seasonal variation of moisture content in unsaturated sandstone inferred from borehole radar and resistivity profiles, Journal of hydrology, 267, 160-172.

Brielmann, H., Griebler, C., Schmidt, S.I., Michel, R., Lueders, T., 2009. Effects of thermal energy discharge on shallow groundwater ecosystems. FEMS Microbiology Ecology, 68, 273-286.

Brouyère, S., 2001. Etude et modélisation du transport et du piégeage des solutés en milieu souterrain sariablement saturé, PhD Thesis, University of Liege, unpublished.

Bruno, P.P.G., Paoletti, V., Grimaldi, M., Rapolla, A., 2000. Geophysical exploration for geothermal low enthalpy resources in Lipari Island, Italy. Journal of volcanology and geothermal research, 98, 173-188.

Busby, J., Lewis, M., Reeves, H., Lawley, R., 2009. Initial geological considerations before installing ground source heat pump systems. Quarterly Journal of engineering geology and hydrogeology, 42, 295-306.

Caterina, D., Beaujean, J., Robert, T., Nguyen, F., 2013. A comparison study of different image appraisal tools for electrical resistivity tomography, Near Surface Geophysics,11 (6), 639-657, doi: 10.3997/1873-0604.2013022 .

Dassargues, A., 1997. Modeling baseflow from an alluvial aquifer using hydraulic-conductivity data obtained from a derived relation with apparent electrical resistivity. Hydrogeology Journal, 5(3), 97-108.

de Groot-Hedlin, C., Constable, S., 1990. Occam’s inversion to generate smooth, two dimensional models from magnetotelluric data. Geophysics, 55, 1613-1624.

de Paly, M., Hecht-Méndez, J., Beck, M., Blum, P., Zell, A., Bayer, P., 2012. optimization of energy extraction for closed shallow geothermal systems using linear programming. Geothermics, 43, 57-65. doi: 10.1016/j.geothermics.2012.03.001

Derouane, J., Dassargues, A., 1998. Delineation of groundwater protection zones based on tracer tests and transport modelling in alluvial sediments. Environmental Geology, 36 (1-2), 27-36.

Doetsch, J.A., Coscia, I., Greenhalgh, S., Linde, N., Green, A., Günther, T., 2010. The borehole-fluid effect in electrical resistivity imaging. Geophysics, 75(4), F107-F114. doi: 10.1190/1.3467824

Garg, S.K., Pritchett, J.W., Wannamaker, P.E., Combs, J., 2007. Characterization of geothermal reservoirs with electrical surveys: Beowave geothermal field. Geothermics, 36, 487-517.

Giambastiani, B.M.S., Colombanii, N., Mastrocicco, M., 2012. Limitation of using heat as a groundwater tracer to define aquifer properties: experiment in a large tank model, Environmental Earth Sciences, published online December 2012, doi: 10.1007/s12665-012-2157-2

Haehnlein, S., Bayer, P., Blum, P., 2010. International legal status of the use of shallow geothermal energy. doi: 10.1016/j.rser.2010.07.069

Haffen, S., Geraud, Y., Diraison, M., Dezayes, C., 2013. Determination of fluid-flow zones in a geothermal sandstone reservoir using thermal conductivity and temperature logs. Geothermics, 46, 32-41.

Hayley, K., Bentley, L.R., Gharibi, M., Nightingale, M., 2007. Low temperature dependence of electrical resistivity: Implications for near surface geophysical monitoring. Geophysical research letters, 34, L18402, doi: 10.1029/2007GL031124**.**

Hermans, T., Caterina, D., Nguyen, F. 2014. Case studies of prior information in electrical resistivity tomography: comparison of different approaches. Near Surface Geophysics, in press.

Hermans T., Daoudi M., Vandenbohede A., Robert T., Caterina D., and Nguyen F. 2012a. Comparison of temperature estimates from heat transport model and electrical resistivity tomography during a shallow heat injection and storage experiment, 1st

International Workshop on Geoelectrical Monitoring, Vienna, Berichte der Geologischen Bundesanstalt, 93, 43-48.

Hermans T., Vandenbohede, A., Lebbe, L., Nguyen, F., 2012b. A shallow geothermal experiment in a sandy aquifer monitored using electric resistivity tomography. Geophysics 77(1), B11-B21, doi:10.1190/GEO2011-0199.1.

Hermans, T., Vandenbohede, A., Lebbe, L., Martin, R., Kemna, A., Beaujean, J., Nguyen, F., 2012c. Imaging artificial salt water infiltration using electrical resistivity tomography constrained by geostatistical data. Journal of Hydrology, 438-439, 168-180, doi:10.1016/j.jhydrol.2012.03.021.

Irving, J., Singha, K. 2010. Stochastic inversion of tracer test and electrical geophysical data to estimate hydraulic conductivities. Water Resources research, 46, W11514.

Jesuβek, A., Grandel, S., Dahmke, A., 2013. Impacts of subsurface heat storage on aquifer hydrogeochemistry. Environmental Earth Sciences, 69 (6), 1999-2012, doi:10.1007/s12665-012-2037-9

Karaoulis, M.C., Kim, J.H., Tsourlos, P.I., 2011. 4D active time constrained resistivity inversion. Journal of Applied Geophysics 73, 25-34. doi:10.1016/j.jappgeo.2010.11.002

Karaoulis, M., Tsourlos, P., Kim, J.-H., Revil, A. 2014. 4D time-lapse ERT inversion: introducing combined time and space constraints. Near surface geophysics, 12, 25-34. Doi:10.3997/1873-0604.2013004.

Kemna, A., 2000. Tomographic inversion of complex resistivity : theory and application. PhD Thesis. University of Bochum.

Kemna, A., Vanderborght, J., Kulessa, B., Vereecken, H., 2002. Imaging and characterization of subsurface solute transport using electrical resistivity tomography (ert) and equivalent transport models. Journal of hydrology, 267, 125-146.

Koestel, J., Kemna, A., Javaux, M., Binley, A., Vereecken, H., 2008. Quantitative imaging of solute transport in an unsaturated and undisturbed soil monolith with 3-D ERT and TDR. Water Resources Research, 44, W12411, doi:10.1029/2007WR006755.

LaBrecque, D.J., Miletto, M., Daily, W., Ramirez, A., Owen, E., 1996a. The effects of noise on Occam's inversion of resistivity tomography data. Geophysics, 61, 538-548. doi: 10.1190/1.1443980.

LaBrecque, D.J., Ramirez, A.L., Daily, W.D., Binley, A.M., Schima, S.A., 1996b. ERT monitoring of environmental remediation processes. Measurement science and technology, **7**, 375-383. doi: 10.1088/0957-0233/7/3/019.

LaBrecque, D.J., Yang, X., 2000. Difference inversion of ERT data: a fast inversion method for 3-D in-situ monitoring. Proc. Symp. Appl. Geophys. Engng Environ. Problems, Environ. Engng Geophys. Soc., 723–732.

Leaf, A.T., Hart, D.J., Bahr, J.M., 2012. Active thermal tracer tests for improved hydrostratigraphic characterization. Ground water, 50 (5), 726-735.

Liang, J., Yang, Q., Liu, L., Li, X., 2011. Modeling and performance evaluation of shallow ground water heat pumps in Beijing plain, China. Energy and Buildings, 43, 3131-3138. doi: 10.106/j.enbuild.2011.08.007

Lo Russo, S., Civita, M. V., 2009. Open-loop groundwater heat pumps development for large buildings: a case study. Geothermics, 38, 335-345. doi: 10.1016/j.geothermics.2008.12.009

Mattsson, N., Steinmann, G., Laloui, L., 2008. Advanced compact device for the in situ determination of geothermal characteristics of soils. Energy and Buildings, 40, 1344-1352.

Miller, C., Routh, P., Brosten, T., McNamara, J. 2008. Application of time-lapse ERT imaging to watershed characterization. Geophysics, 73(3), G7-G17.

Molson, J.W., Frind E.O., Palmer, C.D., 1992. Thermal energy storage in an unconfined aquifer 2. Model development, validation and application. Water resources research, 28, 2857-2867.

Nguyen, F., Kemna, A., Antonsson, A., Engesgaard, P., Kuras, O., Ogilvy, R., Gisbert, J., Jorreto, S., Pulido-Bosch, A., 2009. Characterization of seawater intrusion using 2D electrical Imaging. Near surface geophysics, 7, 377-390.

Nguyen, F., Kemna, A., Robert, T., Hermans, T., Daoudi, M., Flores-Orozco, A., 2011. Inversion of multi-temporal geoelectrical data sets: insights from several case studies, 1st Workshop on Geoelectrical monitoring, GELMON, Vienna, Austria.

Nimmer, R.E., Osiensky, J.L., Binley, A.M., Williams, B.C., 2008. Three-dimensional effects causing artifacts in two-dimensional, cross-borehole, electrical imaging. Journal of hydrology, 359, 59-70. doi: 10.1016/j.hydrol.2008.06.022.

Palmer, C.D., Blowes, D.W., Frind, E.O., Molson, J.W., 1992. Thermal energy storage in an unconfined aquifer 1. Field injection experiment ; Water resource research, 28, 2845-2866.

Pérez Flores, M. A., Gomez Trevino, E., 1997. Dipole-dipole resistivity imaging of the Ahuachapan-Chipilapa geothermal field, El Salvador. Geothermics, 26, 657-680.

Perri, M.T., Cassiani, G., Gervasio, I., Deiana, R., Binley, A., 2012; A saline tracer test monitored via both surface and cross-borehole electrical resistivity tomography: Comparison of time-lapse results. Journal of applied geophysics, 79, 6-16.

Prevedel, B., Wohlgemuth, L., Legarth, B., Henninges, J., Schütt, H., Schmidt-Hattenberger, C., Norden, B., Förster, A., Hurter, S., 2009. The CO_2SINK boreholes for geological CO_2-storage testing. Energy Procedia, 1, 2087-2094. doi: 10.1016/j.egypro.2009.01.272.

Ramirez, A., Daily, W., LaBrecque, D., Owen, E., Chesnut, D., 1993. Monitoring an underground steam injection process using electrical resistance tomography. Water resources research, 29, 73-87.

Raymond, J., Therrien, R., Gosselin, L., Lefebvre, R., 2011. A review of thermal response test analysis using pumping test concepts. Ground Water, 49, 932-945. doi: 10.1111/j.1745-6584.2010.00791.x.

Revil, A., Cathles, L.M., Losh, S., Nunn, J.A., 1998. Electrical conductivity in shaly sands with geophysical applications. Journal of geophysical research, 103, 23925-23936.

Revil, A., Linde, N., 2006. Chemico-electrochemical coupling in microporous media. Journal of colloid and interface science, 302, 682-694.

Revil, A., Skold, M., Karaoulis, M., Schmutz, M., Hubbard, S.S., Mehlhorn, T.L., Watson, D.B. 2013. Hydrogeophysical investigations of the former S-3 ponds contaminant plumes, Oak Ridge Integrated Field Research Challenge site, Tennessee. Geophysics, 78(4), EN29-EN41. Doi: 10.1190/geo2012-0177.1

Robert T., Caterina D., Deceuster J., Kaufmann O., and Nguyen F. 2012. A salt tracer test monitored with surface ERT to detect preferential flow and transport paths in fractured/karstified limestones. Geophysics 77, B55-B67.

Robert, T., Hermans, T., Dumont G., Nguyen, F., Rwabuhungu, D., 2013. Reliability of ERT-derived temperature: insigths from laboratory measurements. Extended Abstract Tu-2Sa-10, Near Surface Geosciences 2013, 11-13 September 2013, Bochum, Germany.

Saar, M.O., 2011. Review: Geothermal heat as a tracer of large-scale groundwater flow and as a means to determine permeability fields. Hydrogeology Journal, 19, 31-52. doi: 10.1007/s10040-010-0657-2.

Sen, P.N., Goode, P.A. 1992. Influence of temperature on electrical conductivity on shaly sands. Geophysics, 46, 781-795.

Sherrod, L., Sauck, W., Werkema, D.D. Jr., 2012. A low-cost, in-situ resistivity and temperature monitoring system, Ground water monitoring & remediation, 32, 31-39. doi: 10.1111/j1745-6592.2011.01380.x

Slater, L., Binley, A.M., Daily, W., Johnson, R., 2000. Cross-hole electrical imaging of a controlled saline tracer injection. Journal of applied geophysics, 44, 85-102.

Tikhonov, A.N., Arsenin, V.A., 1977. Solution of ill-posed problems. Winston & Sons, Washington.

Vandenbohede, A., Louwyck, A., Lebbe, L., 2009. Conservative solute versus heat transport in porous media during push-pull tests. Transport in porous media, 76, 265-287.

Vandenbohede, A., Hermans, T., Nguyen, F., Lebbe, L., 2011. Shallow heat injection and storage experiment: heat transport simulation and sensitivity analysis. Journal of hydrology, 409, 262-272.

Vandenborght, J., Kemna, A., Hardelauf, H., Vereecken, H., 2005. Potential of electrical resistivity tomography to infer aquifer transport characteristics from tracer studies: A synthetic case study. Water Resources research, 41, W06013. doi:10.1029/2004WR003774.

Vanhoudt, D., Desmedt, J., Van Bael, J., Robeyn, N., Hoes, H., 2011. An aquifer thermal storage system in a Belgian hospital: Long-term experimental evaluation of energy and cost savings. Energy and Buildings, 43, 3657-3665. doi: 10.1016/j.enbuild.2011.09.040.

Vereecken, H., Binley, A., Cassiani, G., Revil, A., Titov, K., 2006, Applied Hydrogeophysics, Nato Science Series, IV Earth and Environmental Sciences, 71, Springer.

Warner, D.L., Algan, U., 1984. Thermal impact of residential ground-water heat pumps. Ground water, 22, 6-12.

Zhou, B., Greenhalgh, S.A., 2000. Cross-hole resistivity tomography using different electrode configurations. Geophysical Prospecting, 48, 887-912.

FIGURE

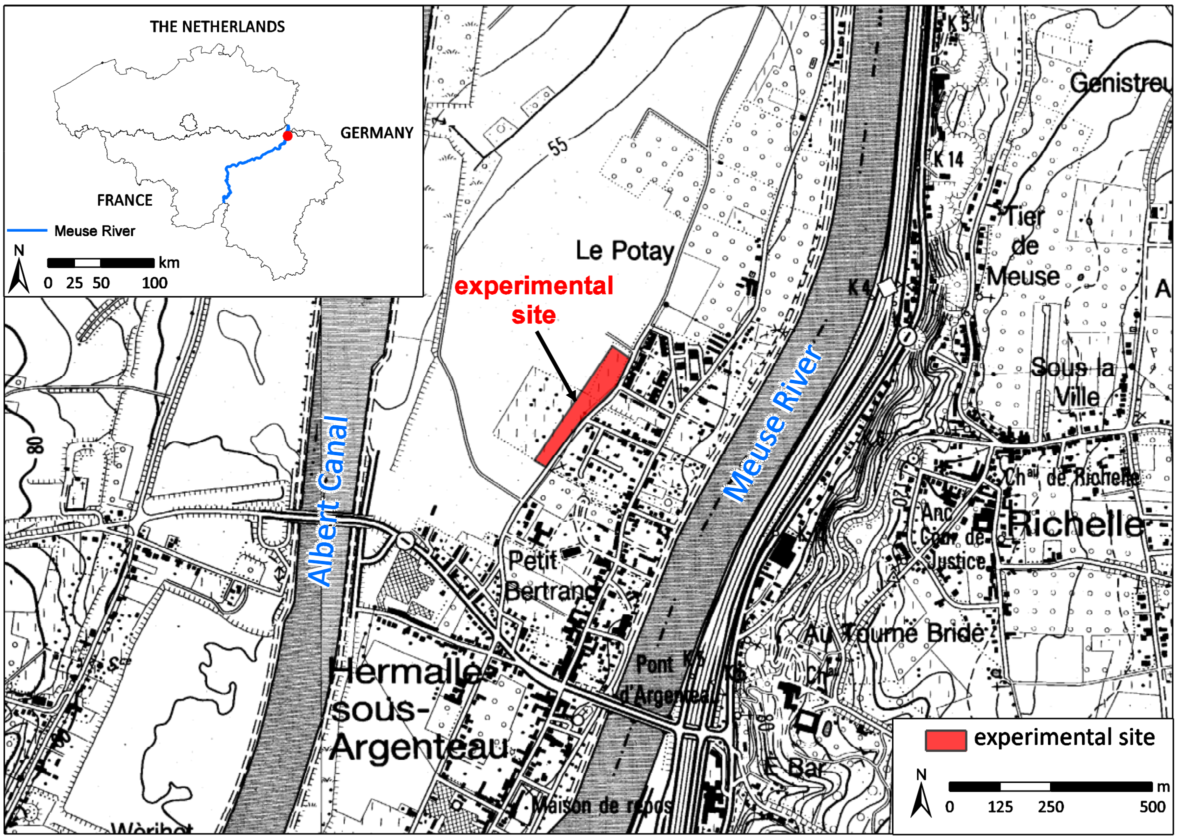

Figure 1. The site of Hermalle-sous-Argenteau is located at the northern part of the Meuse River in Belgium (Wallonia) near the Dutch boarder. It is located almost at mid-distance between the Meuse River and the Albert Canal.

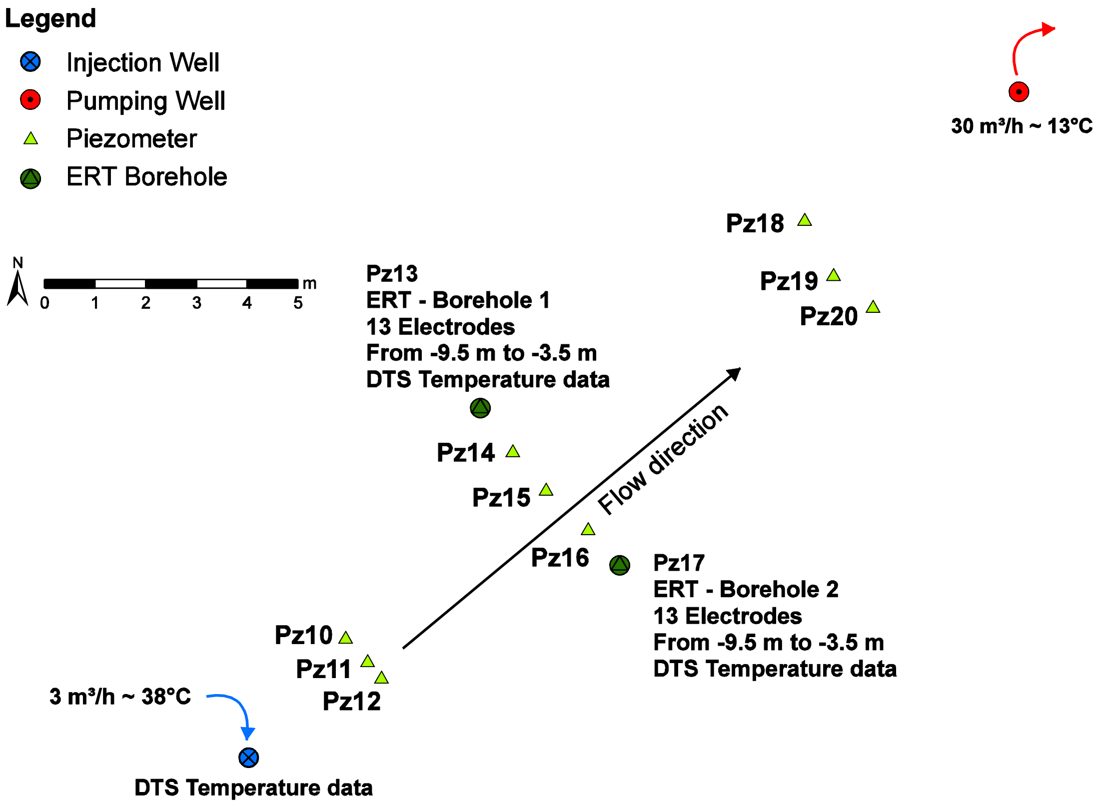

Figure 2. The new piezometers are arranged in three different panels crossing the expected flow direction between an injection and a pumping well. Pz 10-12, Pz, 14-16 and Pz 18-20 are equipped with groundwater temperature loggers at two different levels. On the middle panel, the outer piezometers were equipped with a DTS system and with electrodes.

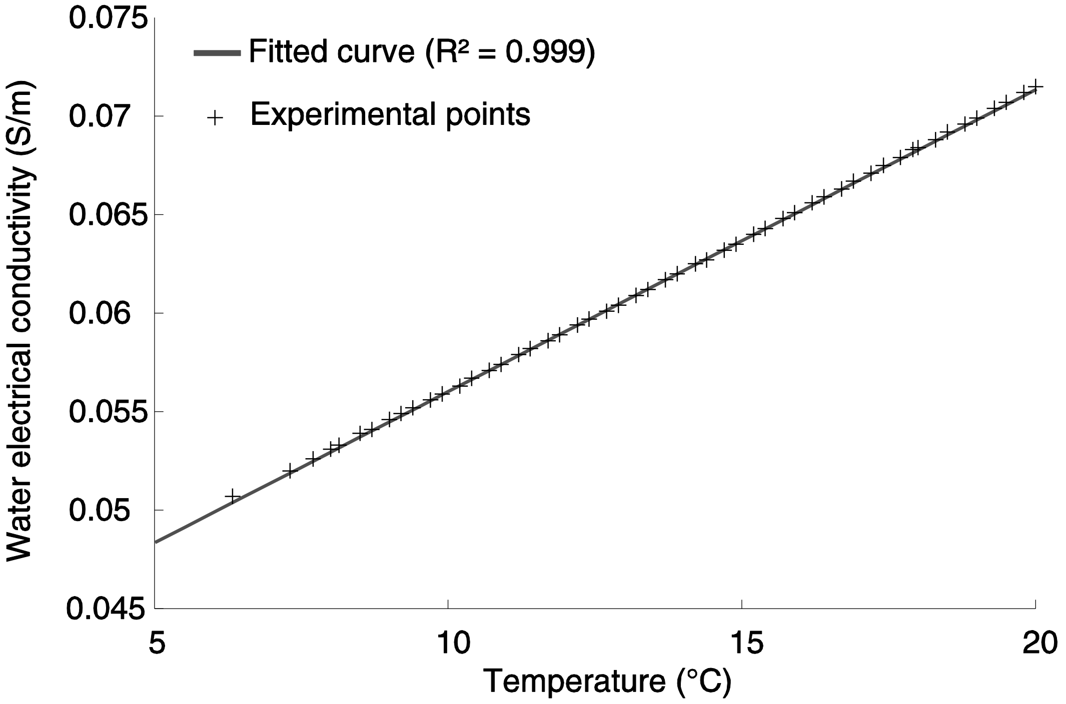

Figure 3. The water electrical conductivity of formation water increases linearly with temperature (points). Parameters of equation 4 were fitted with a fractional change per degree Celsius, m_f, equal to 0.0194 $°C^{-1}$ and the electrical conductivity at 25°C is 0.0791 S/m.

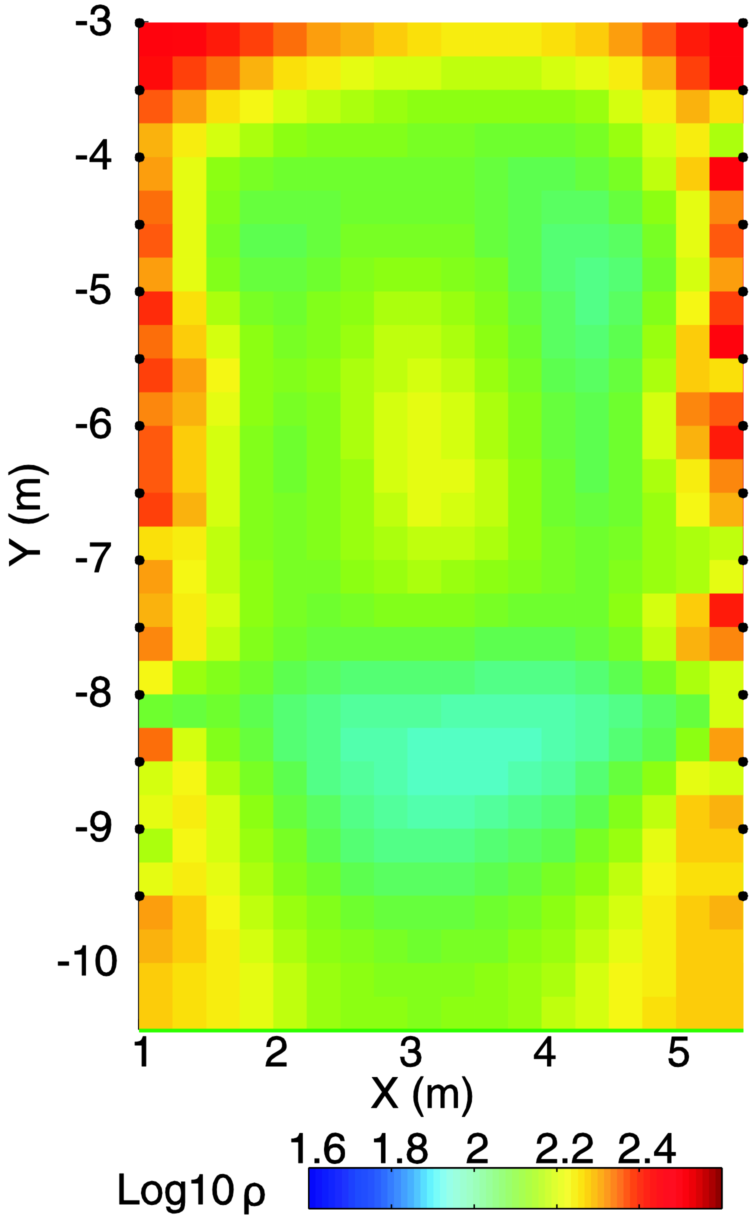

Figure 4. The background inverted section shows resistivity values (Ohm-m) varying between 100 and 200 Ohm-m. The section seems slightly heterogeneous.

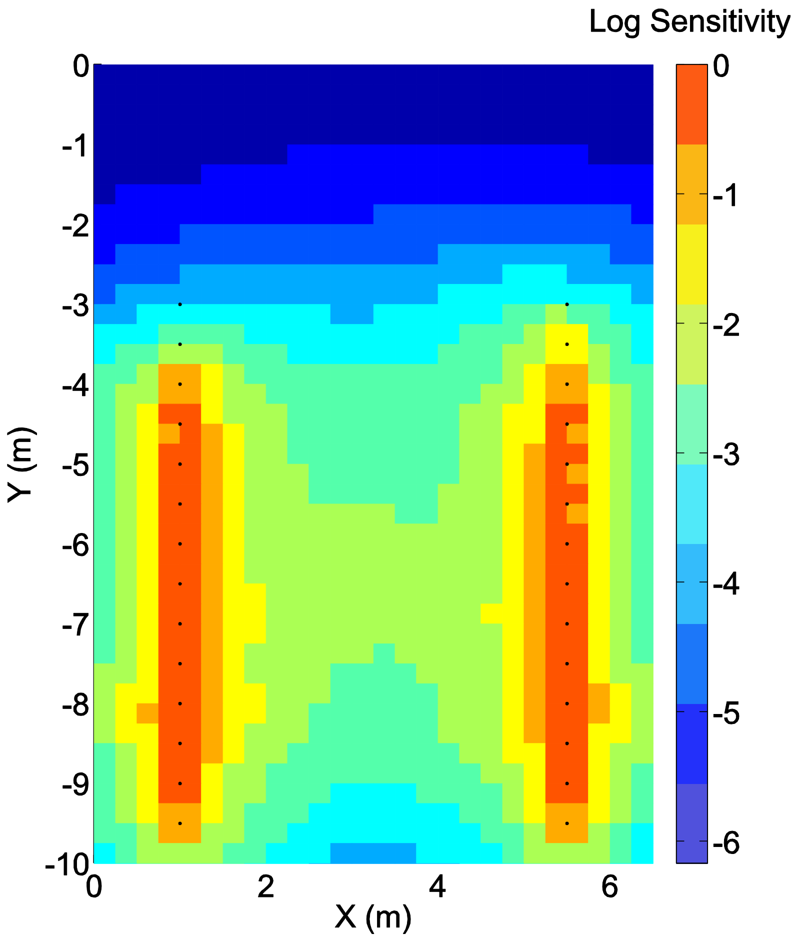

Figure 5. The relative sensitivity pattern is typical of cross-borehole measurements, with smaller sensitivity values in the middle part of the section, especially at the position of top and bottom electrodes.

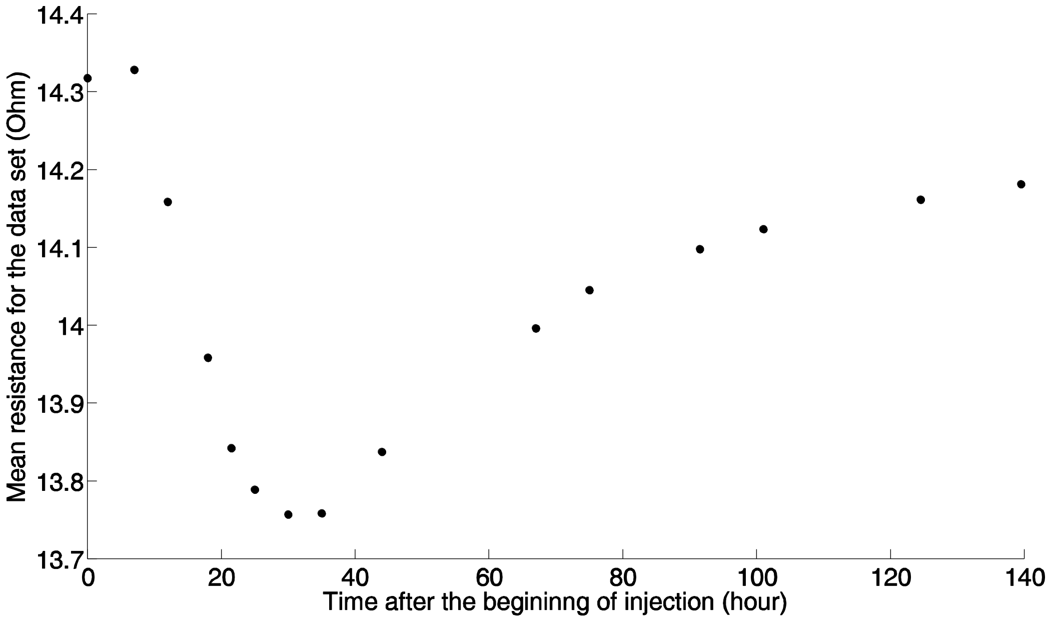

Figure 6. The mean resistance (in Ohm) of the global data set first decreases with depth as the plume of heated water approaches, it reaches a minimum after 30 to 35 hours and then starts to increase slightly.

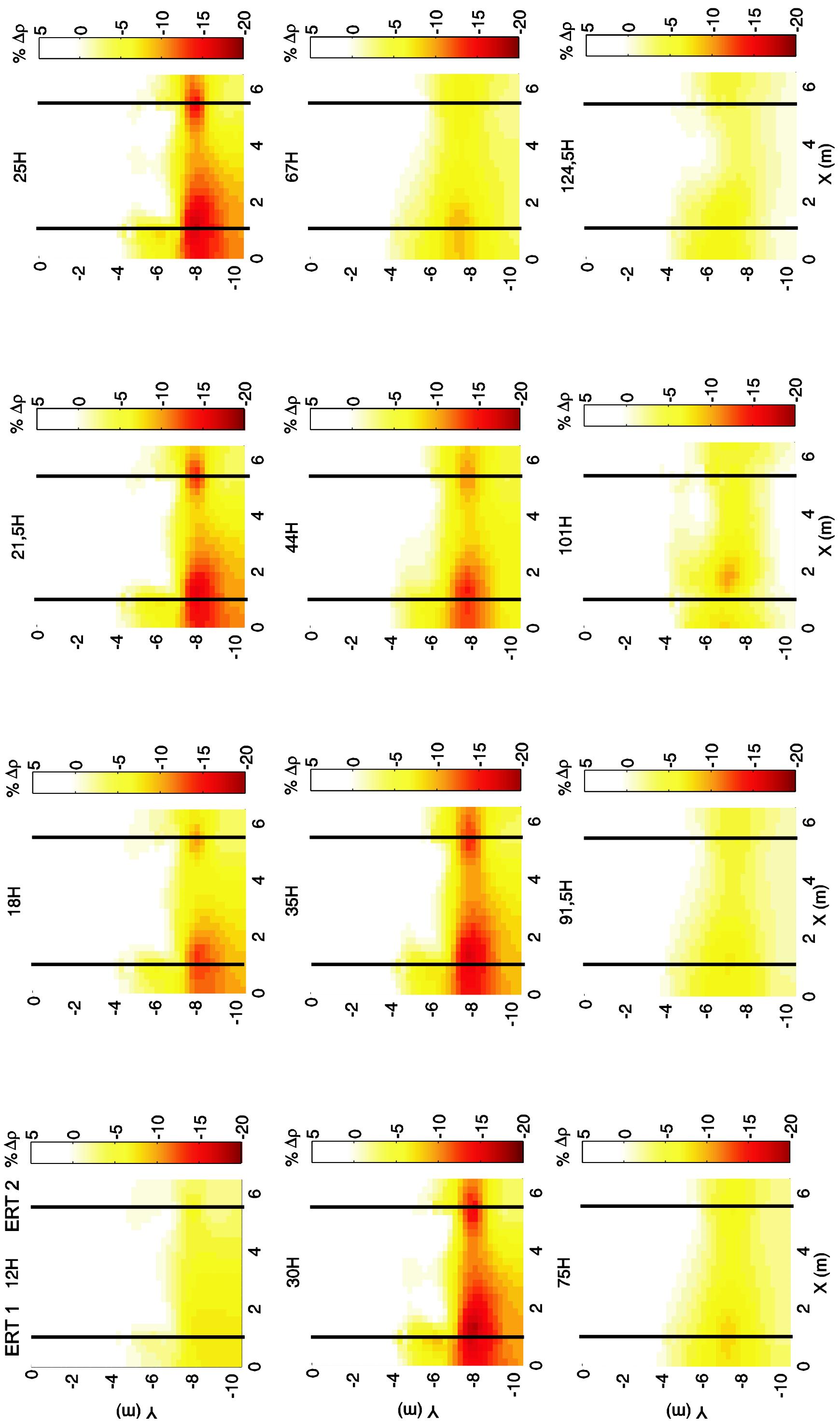

Figure 7. The inverted sections (% change in resistivity) evolve in time with the arrival of the plume. Maximum changes are observed between 30 and 35 h in the surrounding of ERT borehole 1. These sections highlight the spatial heterogeneity of the aquifer. Time is given from the beginning of injection.

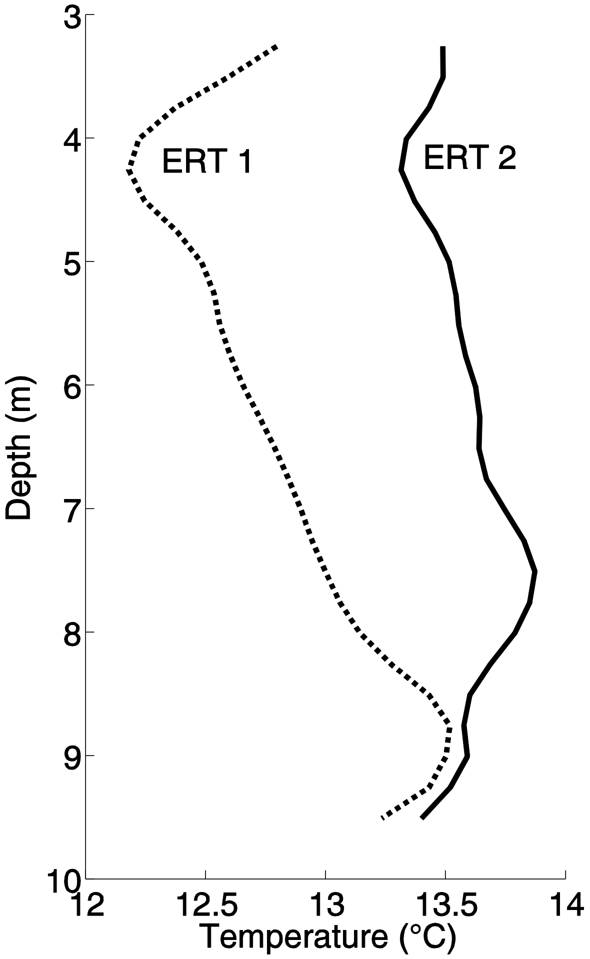

Figure 8. DTS temperature profiles in the two ERT boreholes before the test are not similar. The temperature varies with depth and the mean temperature is different in the two boreholes: 12.8°C in ERT-borehole 1 and 13.6°C in ERT borehole-2.

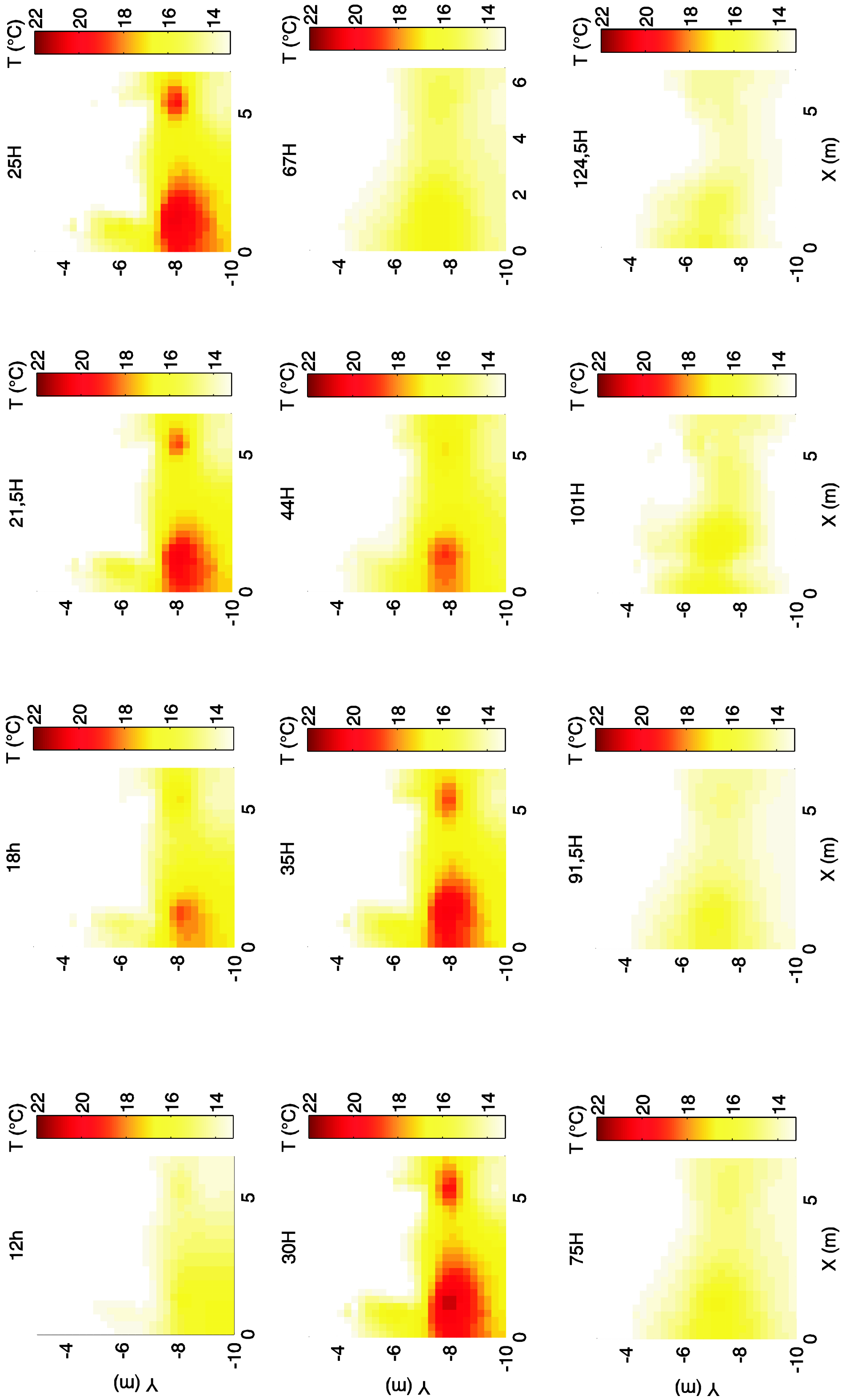

Figure 9. The ERT-derived temperature sections show that the maximum temperature reached is around 21°C in the neighborhood of ERT-borehole 1. The sections are limited to the saturated zone, because equation 5 is not valid in the unsaturated zone.

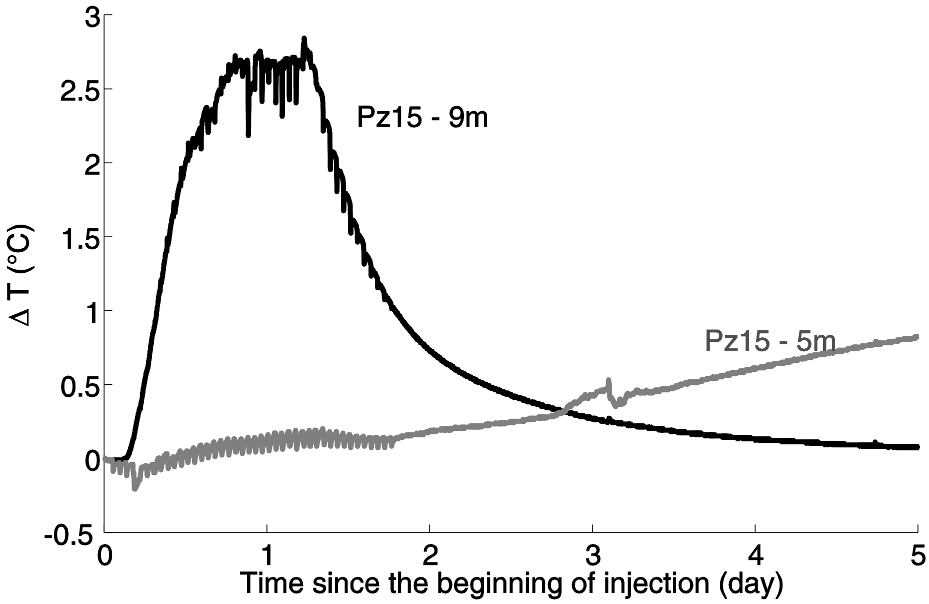

Figure 10. The temperature monitored at two different levels in Pz15 shows that the arrival of the tracers is much quicker and with much higher amplitude in the bottom part of the aquifer than in the upper part.

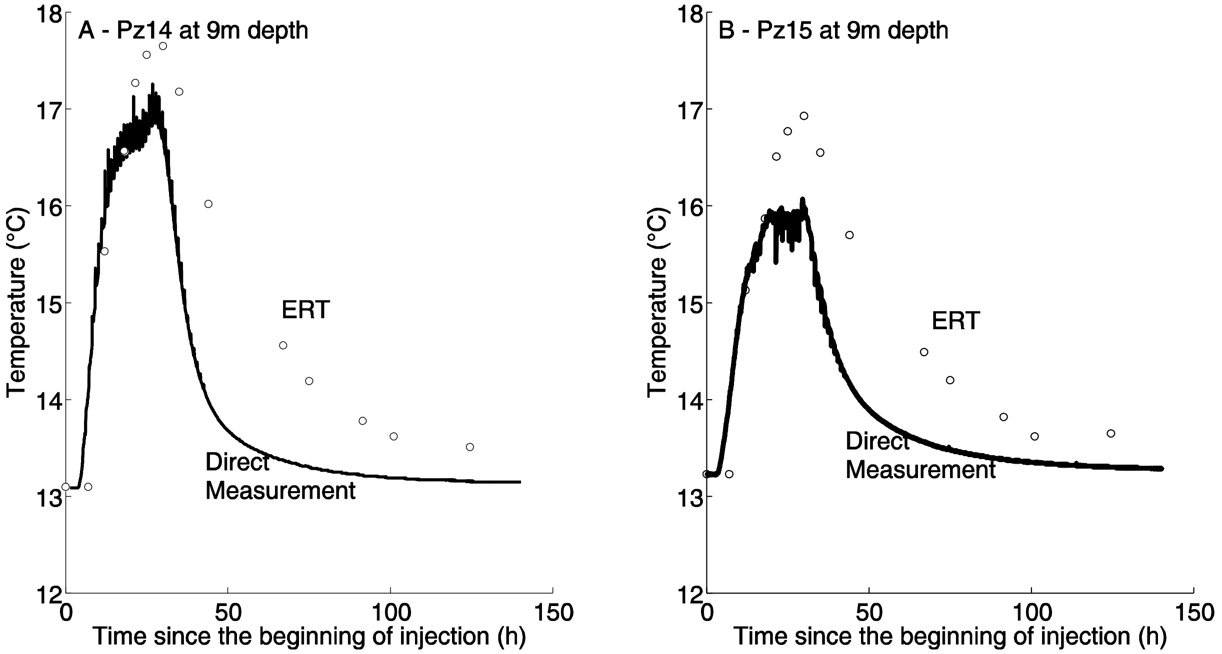

Figure 11. Breakthrough curves for ERT-derived temperatures and direct measurements in Pz14 (A) and Pz15 (B) show a good temporal agreement, but temperature are overestimated for the maximum and the tail of the curve.

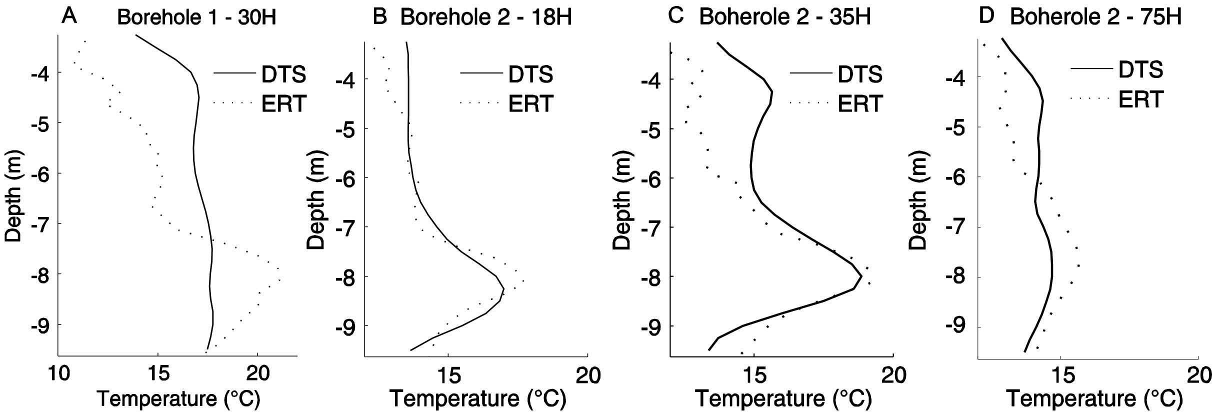

Figure 12. ERT-derived temperature profiles are not consistent with DTS measurements in ERT-borehole 1 (A), but show a very good agreement in ERT-borehole 2 (B, C and D). The almost constant temperature observed with DTS in ERT-borehole 1 may be due to some mixing of water in and around the well.